RoSELS: Road Surface Extraction for 3D Automotive LiDAR Point Cloud Sequence

Dhvani Katkoria and Jaya Sreevalsan-Nair[a]

Graphics-Visualization-Computing Lab (GVCL),
International Institute of Information Technology Bangalore (IIITB), Bangalore, India

Keywords: Road Surface Extraction, 3D LiDAR Point Clouds, Automotive LiDAR, Ego-vehicle, Semantic Segmentation, Ground Filtering, Frame Classification, Road Geometry, Sequence Data, Point Set Smoothing, Range View, Multiscale Feature Extraction, Local Features, Global Features.

Abstract: Road surface geometry provides information about navigable space in autonomous driving. Ground plane estimation is done on "road" points after semantic segmentation of three-dimensional (3D) automotive LiDAR point clouds as a precursor to this geometry extraction. However, the actual geometry extraction is less explored, as it is expensive to use all "road" points for mesh generation. Thus, we propose a coarser surface approximation using road edge points. The geometry extraction for the entire sequence of a trajectory provides the complete road geometry, from the point of view of the ego-vehicle. Thus, we propose an automated system, RoSELS (Road Surface Extraction for LiDAR point cloud Sequence). Our novel approach involves ground point detection and road geometry classification, *i.e. frame classification*, for determining the road edge points. We use appropriate supervised and pre-trained transfer learning models, along with computational geometry algorithms to implement the workflow. Our results on SemanticKITTI show that our extracted road surface for the sequence is qualitatively and quantitatively close to the reference trajectory.

1 INTRODUCTION

Navigable space detection is a challenging problem in robotics and intelligent vehicle technology, which requires an integrated solution from both computer vision and computational geometry. In three-dimensional (3D) automotive LiDAR point cloud processing, *navigable* space implies the ground surface on which a vehicle can traverse, which is predominantly the road surface. Here, the "ground" class of points includes several fine-grained classes, namely, "road," "parking," "sidewalk," "terrain," etc. (Paigwar et al., 2020). The state-of-the-art methods perform ground point segmentation/detection followed by ground plane estimation motivated as a precursor to road surface extraction (Paigwar et al., 2020; Rist et al., 2020). However, we find that ground plane estimation needs to be performed piecewise even for a single point cloud, thus providing a coarse approximation of the surface geometry. Piecewise estimation requires systematic geometric analysis to determine the number, position, and orientation of planes needed to jointly provide a water-tight surface. This is

a challenging point set processing problem, especially as the point clouds are unstructured. Instead, we propose surface mesh extraction from the road points directly. However, generating a fine mesh with all road points is time-consuming. This is alleviated by using an appropriate subset of road points that sufficiently sample the surface. Here, we propose the road edge points and vehicle positions as this desired sample set.

Given we are using the positions of the ego-motion of the vehicle, we can now expand the surface extraction across all frames in a sequence. This leads to creating a watertight road surface for the entire sequence, which is as seen from the point of view of the ego-vehicle. Such a process requires all the point clouds in the sequence, which improves the utilization of the complete dataset.

The conventional data processing workflow for 3D automotive LiDAR point clouds involves semantic segmentation, which readily detects road points. However, the semantic segmentation results have to be post-processed to identify curb or edge points (Behley et al., 2021). At the same time, ground point filtering using local height differences is a reliable solution in the LiDAR point cloud anal-
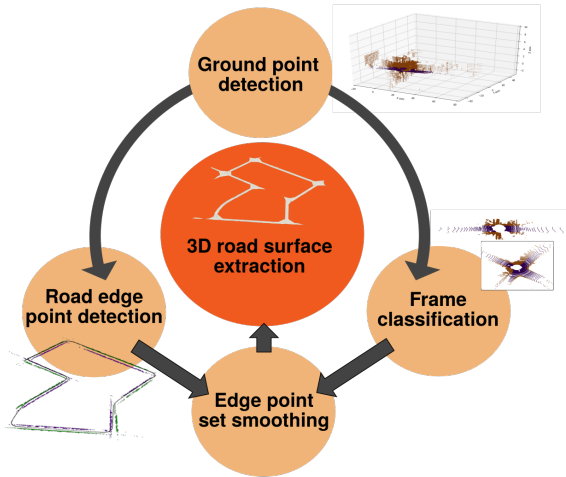
55

Figure 1: Summary of our proposed system, RoSELS, for 3D road surface extraction using ground points detected from an automotive LiDAR point cloud sequence. Our system includes two novel and significant intermediate processes of road edge point detection and frame classification.

ysis (Arora et al., 2021). Binary clustering in point clouds can be done here using highly statistically significant handcrafted features, such as height differences, to classify the points as "edge" and "non-edge" points. Since the expectation-maximization (EM) algorithm has been found to be effective for binary clustering of LiDAR point clouds (Kumari and Sreevalsan-Nair, 2015), we propose a road edge point detection method using binary clustering of ground points. We also use the spatiotemporal locality of the points for outlier removal to improve the ground point detection, and thus the edge points.

Extraction of road geometry becomes challenging in the presence of turnings and complex topology, such as crossroads. Since our work is novel in extracting surface mesh geometry for roads, we first focus on the workflow for straight roads. Such a mesh generation process can be then extended to curved roads, *i.e.* turnings and crossroads. Alternatively, our proposed method can extract contiguous segments of straight roads and fill the gaps between them for short curved segments using surface correction. This solution works for most sequences with a large fraction of contiguous straight roads. For our requirement of identifying contiguous straight roads, the point cloud geometry for each frame needs to be classified. We propose a novel frame-wise point cloud geometry classification, referred to as *frame classification*, using an appropriate image representation of the geometry. We choose an intermediate image representation specifically, as is done in state-of-the-art deep learning classifiers for semantic segmentation (Guo et al., 2020). Here, transfer learning is used

for frame classification.

In summary (Figure 1), our proposed approach is to detect ground points, on which both edge detection and frame classification are performed. We further smooth the edge point set to improve the sample set for surface mesh generation and finally extract the road surface using geometry algorithms. Our novel contributions are in integrating appropriate methods in our proposed system, *RoSELS* (Road Surface Extraction from LiDAR point cloud Sequence) for its implementation (Figure 2). Our key contributions are:

- design and implementation of a complete automated system using ground points, for road surface extraction from the ego-motion in 3D automotive LiDAR point clouds,

- a novel per-frame road-geometry classification, *i.e.* frame classification, using appropriate image representation of the ground points to be used in transfer learning.

- novel use of appropriate point set processing and surface mesh generation methods for performing edge point detection and road surface extraction, respectively.

2 RELATED WORK

The source data for the design of RoSELS is the 3D automotive LiDAR point clouds in the form of sequence based on the trajectory of the ego-motion of the vehicle (Behley et al., 2019; Behley et al., 2021). While most of the existing methods work with frame-wise analysis, the focus here is on the entire sequence. The state of the art in 3D automotive LiDAR point cloud processing on the following topics is relevant to our work:

Ground Point Segmentation: Our starting point for detecting road edge points is ground point segmentation, which is equivalent to point-wise classification into "ground" and "non-ground points." This has been an active area of research since the mid-2000s (Paigwar et al., 2020; Arora et al., 2021). There are two parallel approaches – (i) use height-based handcrafted features and traditional machine learning, and (ii) use convolutional neural networks (CNNs) or convolutional encoder-decoder, either with image representation for its projection (*e.g.* sparse pseudo image, bird's eye view (BEV), range image, etc.) or with 3D points directly (Guo et al., 2020). The latter can be directly used for binary road segmentation (Gigli et al., 2020), specifically. While CNNs work the best for trained environments, they are not as generalized for other environments and are expensive for train-
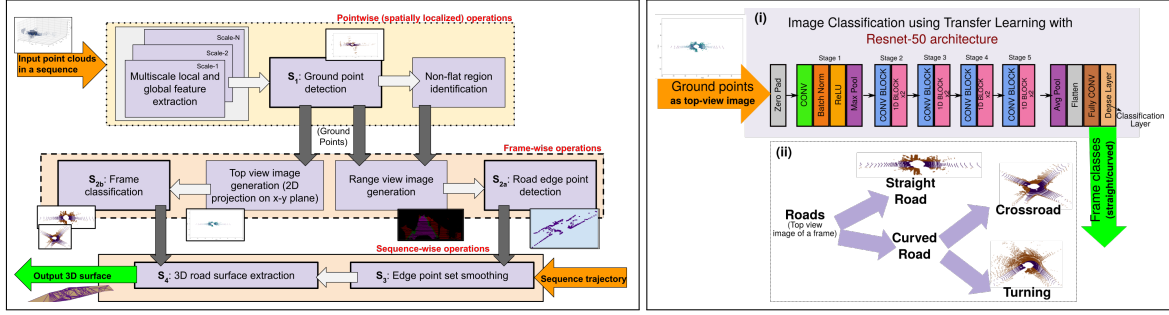
Figure 2: (Left) Our proposed workflow of RoSELS, for generating 3D road surface, from input 3D LiDAR frame-wise point clouds in a sequence and its trajectory information (position and pose of the vehicle). Our workflow is structured and proceeds from point-, frame-, to sequence-wise processing. (Right) Frame classification implemented on top-view images of ground points in each frame, using (i) transfer learning using ResNet-50 architecture (He et al., 2016). The possible class hierarchy for frames is given in (ii), of which we currently focus on the first level of straight and curved road classes.

ing. However, depending on the requirement, height-based feature extraction has been still used for ground point segmentation (Arora et al., 2021; Ouyang et al., 2021). For instance, either geometry-based filtering (Ouyang et al., 2021) or processing of elevation map image (Shen et al., 2021) is done. Such images at various resolutions serve as input to an ensemble edge detection for probabilistic ground point segmentation, through voting (Arora et al., 2021).

An alternative method is the fine-grained multi-class semantic segmentation (Guo et al., 2020), where the appropriate classes can be functionally combined as "ground" class (Paigwar et al., 2020; Arora et al., 2021; Shen et al., 2021). Projection-based methods using deep learning form a widely used class of semantic segmentation methods, for which range images are extensively used (Milioto et al., 2019; Cortinhal et al., 2021). Another set of networks directly use 3D point sample sets, *e.g.* RandLA-Net (Hu et al., 2020), SCSSnet (Rist et al., 2020), etc.

RoSELS uses the lower-cost ground segmentation solution using supervised learning with hand-crafted features, as our goal is to identify the road edge points using the ground segmentation.

Road Edge Extraction: Curb extraction has been studied for mobile laser scanning (MLS)/LiDAR point clouds (Zhao et al., 2021; Sui et al., 2021), monocular images acquired by moving vehicle (Stainvas and Buda, 2014), and elevation map from 2D laser scanner (Liu et al., 2013). All of these methods involve identifying candidate points or positions using elevation filtering and using appropriate line fitting algorithms. Our work is closest to road boundary extraction for MLS point clouds (Sui et al., 2021) where the edge points are located by searching outwards from the vehicle trajectory. The difference, however, is that for the MLS point clouds, the search is performed in the candidate point set, and we exploit the range image view of the vehicle LiDAR point cloud,

on which the search is performed.

In the benchmark SemanticKITTI dataset for vehicle LiDAR point clouds, the curb points are labeled as "sidewalk," where the points are first labeled in tiles by human annotators (Behley et al., 2019), and the road boundary/curb points are then specifically refined (Behley et al., 2021). In the baseline approaches in the benchmark test of semantic segmentation implemented using deep learning architectures, the IoU (intersection over union) score for sidewalk is 75.2% with RangeNet++ (Milioto et al., 2019) and 75.5% in SCSSnet (Rist et al., 2020), which is relatively low.

Thus, we observe that the deep learning solutions for semantic segmentation cater well to classifying road points, but have a gap in road edge point detection. This can be explained by the class imbalance. Hence, we propose a structure-aware method for road edge detection from ground points. Our approach is to detect road edge points using the height-based handcrafted features in supervised learning methods (Arora et al., 2021).

Scene Classification: We look at the state of the art in scene classification, which is the closest to our novel frame classification. Coarse scene classification has been done on satellite or aerial images using transfer learning (Zhou et al., 2018b), where ResNet (Residual Network) (He et al., 2016) has demonstrated near-accurate performance. ResNet with 50 layers (ResNet-50) is optimal in performance and cost for land-cover classification of remote sensing images (Scott et al., 2017). Road type classification based on its functionality as "highway," and "non-highway," has been done on the KITTI vision benchmark suite using AlexNet (Krizhevsky et al., 2012). Since ResNet-50 has worked better on aerial images, we choose to use the same in RoSELS instead of AlexNet, as we require a deep learning architecture that works best for the top-view of the road. The top-views perceptually show a clear distinction between

different road geometry classes, namely the "straight" and "curved" roads.

Ground Plane Estimation: Recent work on road extraction has considered the ground plane estimation and segmentation to be a precursor to the geometry extraction (Paigwar et al., 2020; Rist et al., 2020). GndNet uses 2D voxelization or pillars to generate a pseudo-image which then is passed on to a convolutional encoder-decoder to estimate ground elevation (Paigwar et al., 2020). SCSSnet uses semantic segmentation to identify ground points and performs a simple ground plane estimate (Rist et al., 2020). Since our goal is to perform coarse geometry extraction directly, we identify edge points and triangulate them along with trajectory points. RoSELS is also different from the *mesh map*, which is a triangulation of an automotive LiDAR point cloud using surface normals derived from range images (Chen et al., 2021).

3 PROPOSED WORKFLOW & IMPLEMENTATION

We propose a novel workflow to extract approximate road geometry, for straight roads. The workflow of RoSELS consists of five key steps, namely, (S_1) ground point detection, (S_{2a}) frame classification implicitly giving the road geometry, (S_{2b}) road edge point detection, (S_3) edge point set smoothing, and (S_4) 3D road surface extraction. As shown in Figures 1 and 2:

- S_1 is a point-wise operation, *i.e.* it is implemented on each point in the point cloud, *i.e.* a frame.

- The frame-wise operations, S_{2a} and S_{2b}, are decoupled and implemented in parallel.

- S_3 and S_4 are sequence-wise operations, and hence requires the trajectory information of the vehicle for the entire sequence.

The overall workflow of RoSELS, *i.e.* S_1 to S_4, is captured in Algorithm 1. The partial workflows of the point-wise classification process (S_1) and the sequence-wise road edge extraction (S_{2a}, S_{2b}, S_3) are given in Algorithms 2 and 3, respectively. Our proposed road surface extraction gives the surface as visible from the point-of-view of the vehicle. Hence, the vehicle is called an *ego-vehicle* (Rist et al., 2020).

S_1 – Ground Point Detection: The point cloud is classified into "ground" and "non-ground" points for ground point detection, for which the motivation is explained in Section 2. S_1 involves two sequential substeps, namely, outlier removal and semantic segmentation. Here, we exploit the temporal and spatial locality of the points.

Outlier Removal – Point cloud registration or scan matching, which is widely implemented using the Iterative Closest Point (ICP) registration (Besl Paul and McKay, 1992), is performed on two different point clouds to find the correspondence pairs of points between the two. A correspondence pair implies that there exists an affine transformation (e.g., scaling, rotation and translation) to make a point in one cloud equivalent to a point in the other cloud.

The registration uses temporal locality, *i.e.* points in a frame must be preserved in consecutive frames. Thus, we find correspondence pairs of points in consecutive frames and mark the remaining points as "outliers" to be filtered out. Owing to the continuity of motion across frames, iterative registration on three consecutive frames is implemented at a time. For a given current frame x, we perform registration in two steps. In the first step, outliers are removed in frame $(x-1)$, using registration between frames $(x-1)$ and $(x-2)$. Then, the same process is repeated on frame (x), after performing registration between (x) and $(x-1)$.

Semantic Segmentation – Many of the objects corresponding to non-ground points have elevation (z) higher than that of the ground. Hence, height-based features are best suited for differentiating ground points from others (Arora et al., 2021). The "ground" class is a combination of several fine-grained semantic classes pertaining to the ground, thus making it a coarser class. We extract the local and global spatial handcrafted features, and use them in Random Forest Classifier (RFC) (Breiman, 2001) to segment the point cloud to the ground and the non-ground classes.

The feature extraction is implemented on the point cloud in each frame, after outlier removal. Here, we compute multi-scale local height features, for three scales. Multi-scale features, *i.e.* features captured at different spatial resolutions, are known to work better than a single scale for LiDAR point classification using RFC (Weinmann et al., 2014). Here, for each point, we select a hybrid neighborhood search that combines the criteria of the spherical and the k-nearest neighborhoods (knn). Thus, we identify at most k-nearest neighbors (knn) of a point that are within a given distance, r, from the point. The height features used for ground point detection are listed in Table 1. These extracted features are computed and used in an RFC for both training and testing.

S_{2a} – Road Edge Point Detection: The points on the road edges are those ground points that physically interface with the curb/sidewalk (Behley et al., 2021). RoSELS requires extraction of both the left and right banks of the road. Edge detection is a well-studied problem in image processing, where gradient infor-

Table 1: Point-wise features at each scale for ground detection (S_1).

Local Features	Global Features	Global Features
Point-based		Frame-based
Height-based – Difference from max. – Difference from mean – Standard deviation	Height-based – Value (z-coordinate) – Difference from mean (of frame) Position-based – Distance from sensor – Elevation angle θ	Height-based – Difference from mean – Standard deviation

mation is used for identifying the edges in images and is implemented using the widely used three-step process, which includes differentiation, smoothing, and labeling (Ziou and Tabbone, 1998). Applying the same approach as in image processing, the height gradient is used as the characteristic feature to identify the points on road edges.

However, our method of road edge detection is different from the edge detection in images in two salient ways. Firstly, smoothing is needed for only road edge points, and not the entire point cloud, unlike the image smoothing done for edge detection in images. Thus, we perform edge smoothing and labeling steps, which are now jointly referred to as *edge point set smoothing*, on ground points. Secondly, in our case, the road extraction depends on the road geometry information, *i.e.* determined during S_{2b}. Additionally, unlike the differentiation step which is done on a frame, the edge point set smoothing (*i.e.* S_3) requires the information of the sequence trajectory for coordinate system transformation. Thus, the three steps do not follow successively, here. Thus, S_{2a} is exclusively for the differentiation step, and edge point set smoothing and labeling are implemented in S_3.

Height Gradient-based Differentiation – Here, the first-order derivatives or gradients of height values are computed exclusively of the ground points. We propose point clustering for this task with two specific requirements. Firstly, we cluster road points into regions with low and high height-gradient, referred to as "flat" and "non-flat" regions, respectively. Secondly, the features needed for clustering are computed using height differences. Of the hand-crafted features used for semantic segmentation of 3D airborne and terrestrial LiDAR point clouds (Weinmann et al., 2014), we choose the two appropriate height-difference (Δ_z) features, namely, in a local neighborhood, and in the 2D accumulation map. The 2D accumulation map generates local neighborhoods of points projected to xy-plane, within a square of fixed length (*e.g.* 0.25m), centered at the point. For the clustering process, we observe that the clear clusters do not exist in vehicle LiDAR point clouds. The Expectation-maximization (EM) algorithm (Dempster et al., 1977) has been known to work better than the k-means clustering in

such scenarios. The EM algorithm works with an underlying assumption of the existence of a Gaussian Mixture Model (GMM) in the data. Thus, assuming a bimodal data distribution in the 2D feature space, we use the EM algorithm to determine two clusters of points belonging to the flat and non-flat regions.

Projection to Range Images – The edge points fall in the non-flat regions, where those closest to the centerline, *i.e.* the trajectory, are the desired ones. For a frame-wise operation of centerline detection, the range image of the frame is the best representation of the frame to use. The centerline is defined as the column of the range image where the sensor, *i.e.* the ego-vehicle, is positioned. A range image is a dense rasterized representation of the occluded view from the ego-vehicle point. Thus, it is generated as the spherical projection of the points nearest to the ego-vehicle, and the pixels are colored based on the attribute of the nearest point in the pixel. The image resolution is given by the angular resolution in the elevation and azimuthal angles. For instance, the angular resolution for the Velodyne HDL-64E S2[1] that was used for SemanticKITTI data (Behley et al., 2019) acquisition has 64 angular subdivisions (*i.e.* $\approx 0.4^o$) in elevation angle spanning for 26.8^o, and similarly 0.08^o angular resolution for 360° azimuthal angle, which gives a 64×4500 resolution of range images.

Edge Detection – In order to determine the edge points, we propose the use of a *scanline algorithm* on the range image. We first scan the image of size $H \times W$ row-wise, where the key positions relative to the ego-vehicle, in the pixel space, are:

- at P_{cf}, *i.e.* $(0, \frac{W}{2})$, which indicates the centerline column in the front;

- at P_{cbL}, *i.e.* $(0,0)$, which indicates the centerline column in the back (rear), but on the left-side of the ego-vehicle; and

- at P_{cbR}, *i.e.* $(0,W)$, which indicates the centerline column in the back, but on the right-side.

Note that the left and right sides of the ego-vehicle are with respect to its front face. Thus, at each row, the pixels on the centerline columns are used as the reference for scanning the pixels in the row in the appropriate direction, until a pixel containing a non-flat region point is encountered. For front left and right pixels for non-flat region points, we traverse from P_{cf} towards P_{cbL} and P_{cbR}, respectively. Similarly, in the rear side, for left side, we traverse from P_{cbL} to P_{cf}, and for right side, from P_{cbR} to P_{cf}. After locating these pixels, their corresponding 3D LiDAR points are to be determined. We refer to these row-wise

---

[1]This information is from the sensor specification sheet as published by the sensor manufacturer.

points as p_{fL}, p_{bL} on the left side, and p_{fR}, p_{bR} on the right side. These points are added to the side-specific sets, EP_L and EP_R, for the left and right sides, respectively in each frame.

In this step, the height differences pertaining to other surface variations on the road, *e.g.* potholes, are disregarded. We visualize the points in EP_L and EP_R and ensure that the edges of other surface artifacts are not labeled as road edge points. This is significant, as the artifact points would adversely impact the performance of RoSELS.

S$_{2b}$ – Frame Classification: The underlying road geometry influences the surface extraction method, as expected. Our proposed approach uses the road edge points for generating triangulated (surface) meshes. The edge points along the road boundary are to be sampled sufficiently for accurate edge extraction. This sampling is dependent on the road curvature.

We first consider a broad classification of "straight" and "curved" roads (Figure 2, (Right)(ii)). We restrict our current work to straight roads for three reasons. Firstly, curved roads need more samples as edge points so that the edges can be extracted with sufficient accuracy, and the sample size is determined using geometric methods. Secondly, to extract the curved road edges piecewise, the larger road topology is not sufficiently captured from the point of view of the ego-vehicle. The road topology for turnings and crossroads involve T- and X-intersections which need to be captured, that is beyond the scope of the current workflow. Thirdly, additional interior road points are needed to extract curved road surfaces appropriately. Addressing these three issues requires an in-depth study which is beyond the scope of our current work. Hence, we show a proof-of-concept for our workflow for straight roads exclusively.

Transfer Learning using ResNet-50 Architecture – For 3D LiDAR point cloud sequence, we observe that each frame distinctly demonstrates the road geometry from its top-view, *i.e.* 2D projection of the points on the x-y plane. To exploit the perceptual differences between frames, we propose the use of transfer learning using ResNet-50. It has been used for an effective scene classification of perceptually distinguishable images (He et al., 2016).

The attribute values of the points are used to render the 2D top-view RGB image using perceptually uniform sequential colormap, *i.e.* the viridis colormap. The sequential colormap is further discretized to a predetermined number of bins, say 5 bins. The ground points detected in **S$_1$** are rendered using the colormap with respect to their remission values. We implement transfer learning with the ResNet50 model on these images (Figure 2(Right)).

Here, pre-trained weights for image classification of ImageNet are used, as per the de facto standard in transfer learning on images.

S$_3$ – Edge Point Set Smoothing: Now, the road edge points identified in **S$_{2a}$** are fitted to form edges. These edges are smoothed owing to the noise in the edges. The smoothing is done separately for the left and right sides of the road to avoid filtering out relevant points. Edge labeling refers to the localization of edges and filtering out false positives. Thus, **S$_3$** includes both smoothing and labeling. The edge processing is implemented in the world coordinate system which contains the entire trajectory of the sequence. Hence, the first substep is the coordinate system transformation.

Local to World Coordinate System Transformation – This transformation ensures that the smoothed edge exists as-is in the 3D world space. Also, the smoothing and transformation operations are *non-commutative*, *i.e.* the order of their implementation has to be strictly maintained. Hence, we now add the trajectory information as an input to the workflow (Figure 2(Left)). This input contains the position and poses of the ego-vehicle at each frame of the sequence. The change in position and pose is represented as transformation matrices. These matrices are applied on the edge points in each frame to transform them to the 3D world space.

Point Set Smoothing and Labeling – The straight road edges are smoothed using the transformed coordinates. We first determine subsequences of frames that form contiguous segments of straight roads. This is implemented separately for the left and right sides. The random sample consensus (RANSAC) line fitting model (Fischler and Bolles, 1981) is applied to each such subsequence. Thus, we get disconnected smooth line segments, that look like dashed lines, on both sides of the road.

S$_4$ – 3D Road Surface Extraction: After smoothing, the road surface is extracted as a triangulated mesh formed with the left and right edge points for each contiguous segment of the straight road. Here, a constrained Delaunay tetrahedralization (Shewchuk, 2002) is implemented and is followed by the extraction of the outer/external surface of the tetrahedral mesh. This generates better quality triangles compared to performing 2D Delaunay triangulation on projections of the 3D points.

Implementation of RoSELS: The RoSELS has been implemented on Intel core i7 CPU with 12 GB of RAM. We have used Open3D library APIs (Zhou et al., 2018a) for point cloud registration in **S$_1$**. For neighborhood computation in **S$_1$** and **S$_3$**, Open3D KDTree has been used. The scikit-learn library APIs (Buitinck et al., 2013) have been used for im-

Input : A sequence S of frame-wise point clouds $\{P(f_i) : 0 \leq i < n_{frames}\}$ with frame f_i at index i

Input : Trajectory information of the sequence $T(S)$

Output: 3D surface mesh of the extracted road R_m

$P_{edge} \leftarrow \{\}$ // Set of edge points in S
for *frame f in S* **do**
    // Ground point detection
    // using Algorithm 2
    $G_p(f) \leftarrow$ ground-point-detection($P(f)$)

    // Frame classification using
    // top-view image as straight- or
    // curved-road
    $TV_{img}(f) \leftarrow$ projection-*xy*-plane($G_p(f)$)
    $road\_type(f) \leftarrow$
    classify-using-transfer-learning($TV_{img}(f)$)

    // Straight-road edge detection
    // using Algorithm 3
    if *road_type(f) is "straight-road"* **then**
        $E_p(f) \leftarrow$
        straight-road-edge-detection($G_p(f)$)
        $P_{edge} \leftarrow P_{edge} \cup E_p(f)$ // Merging all
                             // edge points
    end
end
$R_m \leftarrow$ generate-triangulated-mesh(P_{edge})
return R_m

Algorithm 1: The complete workflow of RoSELS for road surface extraction from a sequence.

plementing the RFC and GMM models in S_1 and S_{2a}, respectively. Frame classification model in S_{2b} has been implemented using Keras APIs (Chollet et al., 2015) and the model has been trained for five epochs. Edge point set smoothing in S_3 has used the RANSAC model from the scikit-image library. PyVista library APIs (Sullivan and Kaszynski, 2019) has been used for geometry computation in S_4.

4 EXPERIMENTS & RESULTS

RoSELS specifically requires an input dataset that has sequence(s) of LiDAR point clouds through a trajectory of the vehicle, and also, sufficient annotations for generating machine learning solutions. In that regard, SemanticKITTI (Behley et al., 2019) serves well as our test data.

Input : Point cloud $P(f)$ at a frame f
Output: Set of ground points $G_p(f)$

$G_p(f) \leftarrow \{\}$ // Set of ground points
for *point p in point cloud $P(f)$* **do**
    // Extraction of all features,
    // as given in Table 1
    for $0 \leq i < n_{scales}$ **do**
        $N_i \leftarrow$ find-local-neighborhood(p, *neighborhood_size*)
    end
    $F_p \leftarrow$ compute-features $(P_i, N_1, \ldots, N_{n_{scales}})$

    // Classification of points as
    // ground or non-ground points
    $type(p) \leftarrow$
    classify-using-Random-Forest-Classifier(F_p)

    // Add ground points to the output
    if *type(p) is "ground"* **then**
        $G_p(f) \leftarrow G_p(f) \cup \{p\}$
    end
end
return $G_p(f)$

Algorithm 2: Ground point detection per frame, *i.e.* S_1.

4.1 Dataset

The SemanticKITTI dataset (Behley et al., 2019) has been published primarily for three benchmark tasks, namely semantic segmentation and scene completion of point clouds using single and multi-temporal scans. Since our work is different from the benchmark tasks, validation is not readily available for the dataset. Given its fit as input to RoSELS, we use SemanticKITTI for our experiments and provide an appropriate qualitative and quantitative assessment.

The SemanticKITTI dataset comprises of over 43,000 scans of which over 21,000 are from the training sequence IDs, 00 to 10. We have used the sequence 08 as the validation/test set, as prescribed by the data providers, thus training our model on the remaining training sequences for our classifier models, *i.e.* RFC model for ground point detection (S_1), and transfer learning model for frame classification (S_{2b}). We have only used every 10th frame of training sequences of SemanticKITTI since frames are captured in 0.1s and our subsampling ensures significant variations in the vehicle environment are captured without incurring high computational costs. We have found that including more overlapping data resulted in increased computation without adding new information.

Overall, the dataset has annotations for 28 distinct classes for the semantic segmentation benchmark task. We consider five such classes, namely

Input : Set of ground points $G_p(f)$ at a frame f with label "straight-road"
Input : Trajectory information of the sequence $T(S)$
Output: Set of road edge points $E_p(f)$

$NF_p(f) \leftarrow \{\}$ `// Set of non-flat region points`
for *point p in $G_p(f)$* **do**
   $A_m \leftarrow$ compute-accumulation-map(p)
   $N_g \leftarrow$ find-local-neighborhood(p, *neighborhood_size*)
   $F_{\Delta z} \leftarrow$ compute-local-height-difference-features(G_p, N_g, A_m)
   $region\_type(p) \leftarrow$ classify-using-GMM($F_{\Delta z}$)   `// Classify as flat or non-flat region`
   if *region_type(p) is "non-flat"* **then**
      | $NF_p(f) \leftarrow NF_p(f) \cup \{p\}$
   end
end

`// Generate range image of size (H,W) using non-flat region points`
$R_{img}(f) \leftarrow$ range-image-generation($NF_p(f), G_p(f), H, W$)
$EP_L \leftarrow \{\}$
$EP_R \leftarrow \{\}$

`// Detect edge points from range image`
for $0 \leq row < H$ **do**
   $P_{cf} \leftarrow (row, \frac{W}{2})$ `// Determine centerline pixel in the front side`
                              `// using the column for sensor`
   $P_{cbL}, P_{cbR} \leftarrow (row, 0), (row, W)$ `// Determine centerline pixel in the back (rear) side`
                              `// using the columns for sensor`
   $p_{fL} \leftarrow$ point-in-pixel-furthest-from-centerline-in-pixel-interval($P_{cf}, [P_{cf}, P_{cbL}]$)
   $p_{fR} \leftarrow$ point-in-pixel-furthest-from-centerline-in-pixel-interval($P_{cf}, [P_{cf}, P_{cbR}]$)
   $p_{bL} \leftarrow$ point-in-pixel-furthest-from-centerline-in-pixel-interval($P_{CRL}, [P_{cbL}, P_{cf}]$)
   $p_{bR} \leftarrow$ point-in-pixel-furthest-from-centerline-in-pixel-interval($P_{CRR}, [P_{cbR}, P_{cf}]$)
   $EP_L \leftarrow EP_L \cup \{p_{fL}, p_{bL}\}$
   $EP_R \leftarrow EP_R \cup \{p_{fR}, p_{bR}\}$
   `// Correct the selected edge points in 3D world space`
   for *point p in* $\{p_{fL}, p_{fR}, p_{bL}, p_{bR}\}$ **do**
      | $p \leftarrow$ transform-using-trajectory-information(p, $T(S)$)
   end
end

`// Postprocessing edges to remove outliers`
$EP_L \leftarrow$ smooth-edge-using-RANSAC-line-fitting(EP_L)
$EP_R \leftarrow$ smooth-edge-using-RANSAC-line-fitting(EP_R)
$E_p(f) \leftarrow EP_L \cup EP_R$
return $E_p(f)$

Algorithm 3: Straight road edge detection per frame, followed by collation of edge points from all frames ($\mathbf{S_{2a}}$, $\mathbf{S_{2b}}$, $\mathbf{S_3}$).

"road," "parking," "sidewalk," "other ground," and "terrain," together as the "ground" class in RoSELS. Thus, the "non-ground" class implies the remaining classes, *i.e.* movable objects, such as "car," "bicycle," etc., and stationary objects, such as, "building," "fence," "vegetation," etc. The curbs of the road are labeled as sidewalk (Behley et al., 2021) and are important in our evaluation.

For the frame classification, we have manually annotated all frames in all training sequences, *i.e.* from 00 to 10, into "straight," "crossroad," and "turning."

4.2 Parameter Setting and Experiments

For multi-scale feature extraction for ground point detection using RFC, hybrid criteria for neighborhood determination have been used for three different scales. We have commonly used the constraint of r of $1m$ for the spherical neighborhood in all the scales, and variable k values for the knn neighborhood, *i.e.* $k = 50, 100, 200$ neighbors. We have systematically experimented with several combinations of neighborhood criteria to arrive at this parameter

Table 2: Specifications of the SemanticKITTI sequences used for training and validation/testing in RoSELS.

Seq. ID	# Frames					Ground truth (GT)			Filtered after outlier removal in S_1	
Training	Total	Used	Straight	Crossroad	Turning	# Points	# "Ground" points	"Road"* (%)	# "Ground" points	"Road"* (%)
00	4,541	455	238	205	12	55,300,603	21,242,723	45.2	20,928,740	45.2
01	1,101	111	69	23	19	11,737,924	6,684,753	**71.8**	6,425,398	**72.0**
02	4,661	467	195	134	138	58,678,800	26,955,344	42.8	26,568,086	42.8
03	801	81	17	48	16	10,038,550	4,563,802	**48.8**	4,485,650	**49.0**
04	271	28	25	3	0	3,518,075	1,816,228	**65.9**	1,779,528	**66.4**
05	2,761	277	172	102	3	34,624,816	14,025,815	40.5	13,802,511	40.5
06	1,101	111	54	57	0	13,567,503	8,417,991	34.1	8,223,230	34.1
07	1,101	111	54	57	0	1,3466,390	5,301,837	**48.1**	5,233,937	**48.2**
09	1,591	160	42	39	79	19,894,193	9,313,682	**45.0**	9,159,419	**45.1**
10	1,201	121	64	32	25	15,366,254	5,608,339	**43.7**	5,487,403	**43.9**
All	**19130**	**1922**	**930**	**700**	**292**	**236,193,108**	**103,930,514**	**45.3**	**102,093,902**	**45.3**
Testing									Filtered and Classified in S_1	
08	4071	408	261	124	23	50,006,369	21,943,921	40.3	20,919,150	**41.1**

* Our annotation of "ground" combines five classes, namely, "road," "parking," "sidewalk," "terrain," and "other ground," as given in SemanticKITTI dataset. Percentage values in columns 9 and 11 give the fraction of ground points in columns 8 and 10, respectively, that are annotated as "Road" in SK. Boldface indicates improvement in retaining road points, thus demonstrating the efficiency of processes in S_1.

setting. Similarly, we have used similar hybrid criteria, *i.e.* $r = 1m$ and $k = 50$ for finding the local neighborhood of ground points for computing height-difference features to be used in the GMM for detecting flat and non-flat regions.

We have used sequences 01, 05, 07, and 08 from the training dataset for road surface extraction. We have also tested our proposed method on sequence 15 from the test dataset. Our results for all the sequences are given in Figure 3. The performance of our edge point set smoothing in S_3 in sequence 07 is demonstrated in Figure 4.

4.3 Results

For each step in our workflow, we perform both qualitative analysis using visualization and appropriate quantitative evaluation.

S_1: **Ground Detection:** The details of the sequences used in our models are given in Table 2. For all training sequences, we observe that the percentage of road points preserved as ground points does not reduce after outlier removal in S_1. This shows the efficiency of our outlier removal process while preserving the "road" points. The results of our ground detection using RFC and different experiments we performed by including multi-scale features and registrations are given in Table 3. The table shows the average accuracy and the mean IoU (mIoU) for ground class across all frames of test sequence 08. We observe that GndNet (Paigwar et al., 2020) has reported an mIoU of 83.6%, but is not comparable here, as their mIoU has been calculated across both the ground and non-ground classes together. Similarly, ground segmentation in (Arora et al., 2021) has reported an mIoU for the "ground" class as 78.46% but it is not comparable as their "ground" class includes "vegetation" additionally. While we cannot directly compare, these mIoU scores indicate that our approach for ground point classification shows a considerably high level

Table 3: Ground detection using random forest classifier (RFC).

Set of points to be classified	# Scales for local features	Classification accuracy (%-age)	mIoU (%-age)
All points	1 (single scale)	96.37	89.38
	3 (multi-scale)	96.63	90.63
Filtered* points	1 (single scale)	96.58	89.47
	3 (multi-scale)	96.91	90.79

* Filtered points are those that were retained after outlier removal in S_1.

Table 4: Results of frame classification using transfer learning.

#Class hierarchy* levels	Class outcomes	Classification accuracy (%age)
1	Straight road, Curved road	82.35
2	Straight road, Crossroad, Turning	78.51

* Frame class hierarchy is as shown in Figure 2(Right,(ii)).

Table 5: Class distribution of road edge points in extracted surface.

GT Class ↓	# Points (% age)			
Seq. ID →	01	05	07	08
Road	12,437 (**94.0**)	10,093 (**63.4**)	3,864 (**76.5**)	19,856 (**84.3**)
Parking	0	408 (2.6)	448 (**8.9**)	710 (3.0)
Sidewalk	6 (**0.0**)	5,243 (**32.9**)	695 (**13.8**)	2,599 (**11.0**)
Terrain	519 (3.9)	161 (1.0)	42 (0.8)	393 (1.7)
Other-ground	276 (2.1)	18 (0.1)	0	0
Non-ground	0	0	0	7 (0.0)

* Underlined %-age values show that road edge points in the extracted surface belong to "road" and "sidewalk" classes, predominantly, and as desired.

of accuracy.

S_{2a}: **Frame Classification:** As an experiment, we have trained two different frame classification models corresponding to the different levels of frame/road geometry class hierarchy (Figure 2, (Right)(ii)). The first model is for classification into straight or curved roads, and the second one is for classification into straight roads, crossroads, and turnings. The validation accuracy on sequence 08 for both the frame classification models is shown in Table 5. Given the higher accuracy at the first level of classification, we have used the model for "straight" and "curved" roads here. These accuracy results can be further improved in future work by addressing the class imbalance in both hierarchical levels (Table 2).
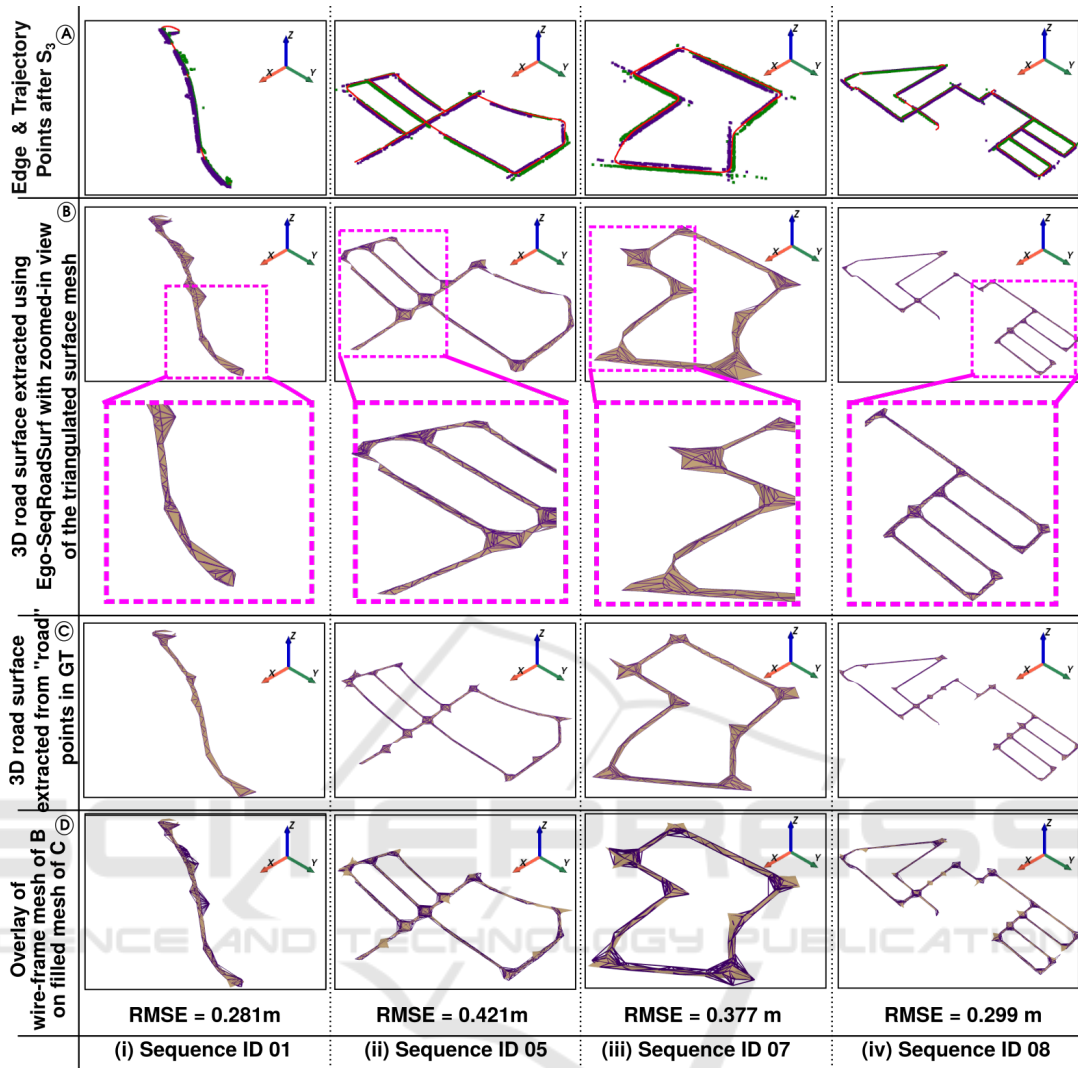
Figure 3: Results of implementing RoSELS on training sequences of SemanticKITTI (Behley et al., 2019), where 01, 05, and 07 have been used for training our learning models, and 08 has been used for validation/testing. Row A follows the color scheme as mentioned in Figure 4. For rows B, C, and D wireframe meshes are shown in indigo and filled meshes are shown in tan color.

S_3: Edge Point Set Smoothing: The class distribution of our road edge points after S_3 is shown in Table 5. We observe that most of the edge points belong to the "road" class predominantly, followed by the "sidewalk" class. This shows that our approach identifies edge points that are annotated as "road" or "sidewalk," as expected. This shows the combined efficiency of S_{2a}, S_{2b}, and S_3. The edge point set smoothing results for sequence 07 in Figure 4 show that the noise in edge points is substantially reduced, thus giving smooth road edges on the left and right of the trajectory.

To quantify the error, we perform these three steps on the "road" points in the ground truth (GT), and compute the root mean square error between the edge

point sets computed using "road" (GT) and "ground" (detected in S_1) points. We perform this analysis owing to the absence of ground truth of edge points and extracted surface. The RMSE values for sequences 01, 05, 07, and 08 are given in Figure 3. Given that each frame has an extent of 51.2m in front of the vehicle and 25.6m on either side (Behley et al., 2019), we observe that the RMSE errors are relatively low.

S_4: 3D Road Surface Extraction: The results of the 3D extracted surface for trajectories of different sequences are visualized in Figure 3. Our qualitative results show that RoSELS works efficiently on straight paths, closed trajectories, and complex trajectories that predominantly have large contiguous segments of straight roads. Our results of surfaces ex-
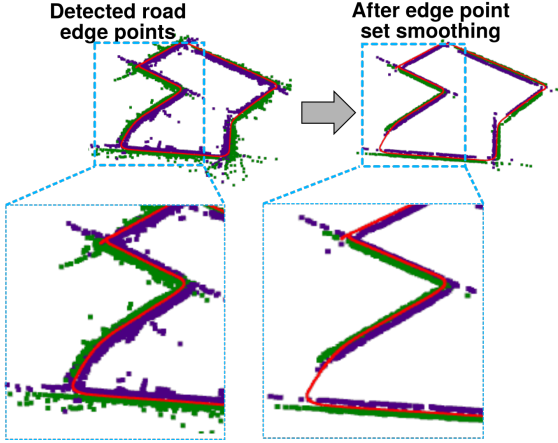
Figure 4: Edge point set smoothing results on sequence 07 data trajectory (top row) with zoomed-in region inset (bottom row). Red, purple and green points show the trajectory, left and right edge points, respectively.
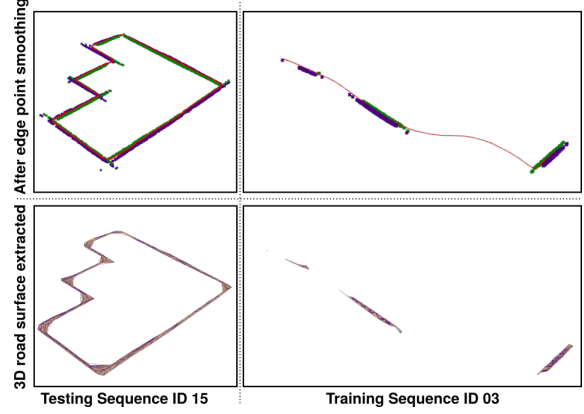

Figure 5: Results of RoSELS on (Left) a sample sequence from the test set of SemanticKITTI (Behley et al., 2019), for which annotations for semantic segmentation have not been published; and (Right) a sample sequence where the surface is only partially extracted.

tracted using detected ground points and "road" (GT) points are overlaid for demonstrating their similarity. It can be seen that short segments of turning or connections between straight road segments have also been effectively covered in the triangulated meshes.

RoSELS has also been entirely implemented on test sequence 15. As the GT for the test sequences is not available, we qualitatively compare our extracted road surface with the reference trajectory using surface and point rendering (Figure 5(Left)). In all sequences, including 15, we observe that the road surface mesh preserves the trajectory as its *medial skeleton* (Tagliasacchi et al., 2016), as expected.

However, RoSELS fails to extract the road surface for the entire trajectory where: (a) the segments with straight roads are highly fragmented, and (b) the subsequences have comparable segments of curved and straight roads. When edge points are not identified for large segments of the road, as seen in training sequence 03 (Figure 5(Right)), RoSELS extracts the road surface partially. Surface extraction for a complete trajectory for such scenarios requires an in-depth study of curved roads, which is beyond the scope of our current work.

5 CONCLUSIONS

We have proposed and implemented RoSELS, a novel system for automating 3D road surface extraction for a sequence of 3D automotive LiDAR point clouds. It implements a five-step workflow. Firstly, with outlier removal and multiscale feature extraction, supervised learning using RFC is used for ground point detection. Secondly, the height differences in ground

points are used to detect road edge points using the EM algorithm. Simultaneously, our frame classification provides the road geometry by transfer learning using ResNet-50 on top-view images. The fourth step is for smoothing the edge point set in the sequence. As the last step, the 3D road surface is extracted as a triangulated mesh using 3D Delaunay tetrahedralization. Our experiments on four sequences in SemanticKITTI with varying complexity in geometry have yielded good results, which have been qualitatively and quantitatively verified. Thus, RoSELS works successfully on trajectories with contiguous straight roads, predominantly.

Although road surfaces across different trajectories are extracted with a high level of visual similarity using the proposed algorithm, our approach fails to extract road surfaces for the entire trajectory where the segments do not have contiguous straight road geometry. Thus, extending our method to curved roads is in the scope of future work. A more robust metric and ground truth for validation are also open challenges for the road surface extraction application.

ACKNOWLEDGEMENT

REFERENCES

Arora, M., Wiesmann, L., Chen, X., and Stachniss, C. (2021). Mapping the Static Parts of Dynamic Scenes from 3D LiDAR Point Clouds Exploiting Ground Segmentation. In *2021 European Conference on Mobile Robots (ECMR)*, pages 1–6. IEEE.

Behley, J., Garbade, M., Milioto, A., Quenzel, J., Behnke, S., Gall, J., and Stachniss, C. (2021). Towards 3d lidar-based semantic scene understanding of 3d point cloud sequences: The semantickitti dataset. *The International Journal of Robotics Research*, 40(8-9):959–967.

Behley, J., Garbade, M., Milioto, A., Quenzel, J., Behnke, S., Stachniss, C., and Gall, J. (2019). SemanticKITTI: A dataset for semantic scene understanding of LiDAR sequences. In *Proceedings of the IEEE/CVF International Conference on Computer Vision*, pages 9297–9307.

Besl Paul, J. and McKay, N. D. (1992). A method for registration of 3-D shapes. *IEEE Transactions on Pattern Analysis and Machine Intelligence*, 14(2):239–256.

Breiman, L. (2001). Random forests. *Machine learning*, 45(1):5–32.

Buitinck, L., Louppe, G., Blondel, M., Pedregosa, F., Mueller, A., Grisel, O., Niculae, V., Prettenhofer, P., Gramfort, A., Grobler, J., Layton, R., VanderPlas, J., Joly, A., Holt, B., and Varoquaux, G. (2013). API design for machine learning software: experiences from the scikit-learn project. In *ECML PKDD Workshop: Languages for Data Mining and Machine Learning*, pages 108–122.

Chen, X., Vizzo, I., Läbe, T., Behley, J., and Stachniss, C. (2021). Range image-based LiDAR localization for autonomous vehicles. In *2021 IEEE International Conference on Robotics and Automation (ICRA)*, pages 5802–5808. IEEE.

Chollet, F. et al. (2015). Keras. https://keras.io.

Cortinhal, T., Tzelepi, G., and Aksoy, E. (2021). SalsaNext: Fast, Uncertainty-aware Semantic Segmentation of LiDAR Point Clouds for Autonomous Driving. In *15th International Symposium, ISVC 2020, San Diego, CA, USA, October 5–7, 2020*, volume 12510. Springer.

Dempster, A. P., Laird, N. M., and Rubin, D. B. (1977). Maximum likelihood from incomplete data via the EM algorithm. *Journal of the Royal Statistical Society: Series B (Methodological)*, 39(1):1–22.

Fischler, M. A. and Bolles, R. C. (1981). Random sample consensus: A paradigm for model fitting with applications to image analysis and automated cartography. *Communications of the ACM*, 24(6):381–395.

Gigli, L., Kiran, B. R., Paul, T., Serna, A., Vemuri, N., Marcotegui, B., and Velasco-Forero, S. (2020). Road Segmentation on low resolution LIDAR point clouds for autonomous vehicles. In *XXIV International Society for Photogrammetry and Remote Sensing Congress*, Nice, France. ISPRS 2020.

Guo, Y., Wang, H., Hu, Q., Liu, H., Liu, L., and Bennamoun, M. (2020). Deep learning for 3d point clouds: A survey. *IEEE transactions on pattern analysis and machine intelligence*.

He, K., Zhang, X., Ren, S., and Sun, J. (2016). Deep residual learning for image recognition. In *Proceedings of the IEEE conference on computer vision and pattern recognition*, pages 770–778.

Hu, Q., Yang, B., Xie, L., Rosa, S., Guo, Y., Wang, Z., Trigoni, N., and Markham, A. (2020). Randla-net: Efficient semantic segmentation of large-scale point clouds. In *Proceedings of the IEEE/CVF Conference on Computer Vision and Pattern Recognition*, pages 11108–11117.

Krizhevsky, A., Sutskever, I., and Hinton, G. E. (2012). Imagenet classification with deep convolutional neural networks. *Advances in neural information processing systems*, 25.

Kumari, B. and Sreevalsan-Nair, J. (2015). An interactive visual analytic tool for semantic classification of 3D urban LiDAR point cloud. In *Proceedings of the 23rd SIGSPATIAL International Conference on Advances in Geographic Information Systems*, pages 1–4.

Liu, Z., Liu, D., Chen, T., and Wei, C. (2013). Curb detection using 2D range data in a campus environment. In *2013 Seventh International Conference on Image and Graphics*, pages 291–296. IEEE.

Milioto, A., Vizzo, I., Behley, J., and Stachniss, C. (2019). Rangenet++: Fast and accurate lidar semantic segmentation. In *2019 IEEE/RSJ International Conference on Intelligent Robots and Systems (IROS)*, pages 4213–4220. IEEE.

Ouyang, Z., Dong, X., Cui, J., Niu, J., and Guizani, M. (2021). PV-EncoNet: Fast Object Detection Based on Colored Point Cloud. *IEEE Transactions on Intelligent Transportation Systems*, Early Access:1–12.

Paigwar, A., Erkent, Ö., Sierra-Gonzalez, D., and Laugier, C. (2020). Gndnet: Fast ground plane estimation and point cloud segmentation for autonomous vehicles. In *2020 IEEE/RSJ International Conference on Intelligent Robots and Systems (IROS)*, pages 2150–2156. IEEE.

Rist, C. B., Schmidt, D., Enzweiler, M., and Gavrila, D. M. (2020). SCSSnet: Learning Spatially-Conditioned Scene Segmentation on LiDAR Point Clouds. In *2020 IEEE Intelligent Vehicles Symposium (IV)*, pages 1086–1093. IEEE.

Scott, G. J., England, M. R., Starms, W. A., Marcum, R. A., and Davis, C. H. (2017). Training deep convolutional neural networks for land–cover classification of high-resolution imagery. *IEEE Geoscience and Remote Sensing Letters*, 14(4):549–553.

Shen, Z., Liang, H., Lin, L., Wang, Z., Huang, W., and Yu, J. (2021). Fast Ground Segmentation for 3D LiDAR Point Cloud Based on Jump-Convolution-Process. *Remote Sensing*, 13(16):3239.

Shewchuk, J. R. (2002). Constrained Delaunay Tetrahedralizations and Provably Good Boundary Recovery. In *Eleventh International Meshing Roundtable (IMR)*, pages 193–204.

Stainvas, I. and Buda, Y. (2014). Performance evaluation

for curb detection problem. In *2014 IEEE Intelligent Vehicles Symposium Proceedings*, pages 25–30. IEEE.

Sui, L., Zhu, J., Zhong, M., Wang, X., and Kang, J. (2021). Extraction of road boundary from MLS data using laser scanner ground trajectory. *Open Geosciences*, 13(1):690–704.

Sullivan, C. B. and Kaszynski, A. (2019). PyVista: 3D plotting and mesh analysis through a streamlined interface for the Visualization Toolkit (VTK). *Journal of Open Source Software*, 4(37):1450.

Tagliasacchi, A., Delame, T., Spagnuolo, M., Amenta, N., and Telea, A. (2016). 3D Skeletons: A State-of-the-Art Report. In *Computer Graphics Forum*, volume 35, pages 573–597. Wiley Online Library.

Weinmann, M., Jutzi, B., and Mallet, C. (2014). Semantic 3D scene interpretation: A framework combining optimal neighborhood size selection with relevant features. *ISPRS Annals of the Photogrammetry, Remote Sensing and Spatial Information Sciences*, 2(3):181. doi : https://doi.org/10.5194/isprsannals-II-3-181-2014.

Zhao, L., Yan, L., and Meng, X. (2021). The Extraction of Street Curbs from Mobile Laser Scanning Data in Urban Areas. *Remote Sensing*, 13(12):2407.

Zhou, Q.-Y., Park, J., and Koltun, V. (2018a). Open3D: A modern library for 3D data processing. *arXiv:1801.09847*.

Zhou, Z., Zheng, Y., Ye, H., Pu, J., and Sun, G. (2018b). Satellite image scene classification via ConvNet with context aggregation. In *Pacific Rim Conference on Multimedia*, pages 329–339. Springer.

Ziou, D. and Tabbone, S. (1998). Edge Detection Techniques - an Overview. *Pattern Recognition and Image Analysis (Advances in Mathematical Theory and Applications)*, 8(4):537–559.